Title
Superplastic Creep of Eutectic Tin-Lead Solder Joints

Authors
Mei, Z.
Hansen, R.
Shine, M.C.
et al.

Publication Date
1990-09-01

Center for Advanced Materials

CAM

To be presented at the 1990 ASME/WAM "Mechanics of Surface Mount Assemblies Symposium," Dallas, TX, November 30, 1990, and to be published in the Proceedings

Superplastic Creep of Eutectic Tin-Lead Solder Joints

Z. Mei, R. Hansen, M.C. Shine, and J.W. Morris, Jr.

September 1990

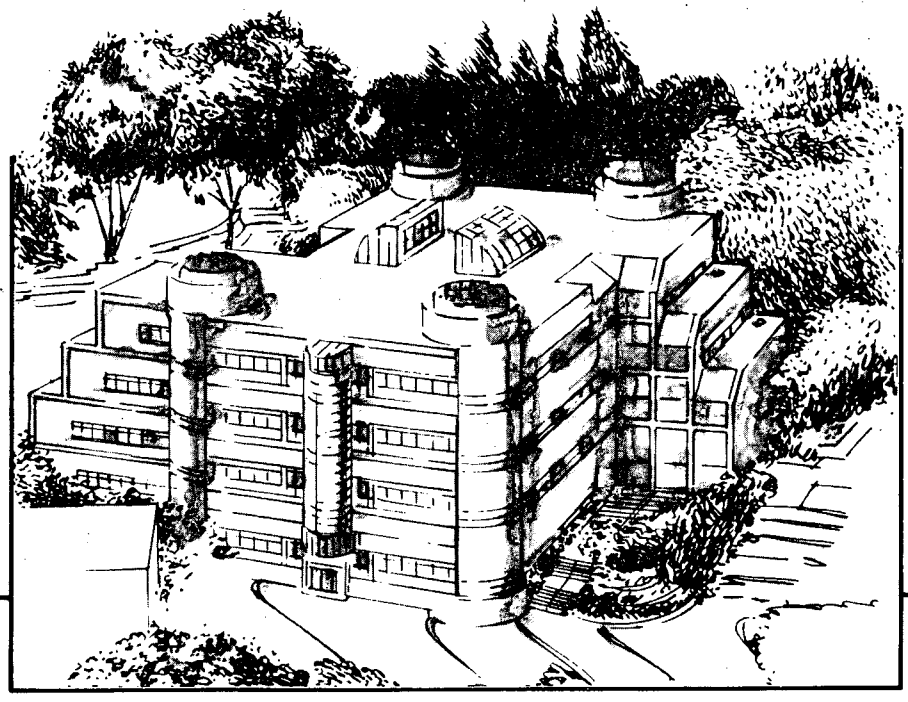

Materials and Chemical Sciences Division

Lawrence Berkeley Laboratory • University of California

ONE CYCLOTRON ROAD, BERKELEY, CA 94720 • (415) 486-4755

Prepared for the U.S. Department of Energy under Contract DE-AC03-76SF00098

DISCLAIMER

Superplastic Creep of Eutectic Tin-Lead Solder Joints

Z. Mei*, R. Hansen*, M. C. Shine+, and J. W. Morris, Jr.*

*Department of Materials Science and Mineral Engineering
University of California
and
*Center for Advanced Materials
Materials and Chemical Sciences Division
Lawrence Berkeley Laboratory
1 Cyclotron Road
Berkeley, CA 94720

and

+Digital Equipment Corporation, Cupertino, CA 95014

September 1990

This work was supported by Digital Equipment Corporation and by the Director, Office of Energy Research, Office of Basic Energy Science, Materials Sciences Division of the U. S. Department of Energy under Contract No. *DE-AC03-76SF00098.* The

Superplastic Creep of Eutectic Tin-Lead Solder Joints

Z. Mei*, R. Hansen*, M. C. Shine+, and J. W. Morris, Jr.*

*Center for Advanced Materials, Lawrence Berkeley Laboratory and
Department of Materials Science and Mineral Engineering, University of California,
Berkeley, CA 94720
+Digital Equipment Corporation, Cupertino, CA 95014

Creep behavior of air-cooled and liquid nitrogen-quenched soldered joints of 60/40 Sn-Pb at 65° C has been studied. The stress exponent, n, in the power law, $\dot{\gamma}$ (steady state strain rate) $\propto \sigma^n$ (applied stress), changes from a value of about 6 to values of 2 or 3, as $\dot{\gamma}$ decreases below 10^{-4} in/in per second. This result, combined with the authors' previous stepped load creep test results, indicates a transition in creep deformation mechanism from conventional dislocation climbing to superplastic grain boundary sliding. The superplastic creep of the soldered joints is ascribed to their non-lamellar microstructure due to their fast cooling rate. During creep deformation, recrystallization of the soldered joints occurs, resulting in a softening phenomenon.

I. INTRODUCTION

Thermal fatigue of solder joints results from the thermal expansion mismatch between soldered materials, and is an increasing reliability concern in microelectronic packaging. Because of its low melting point, a eutectic Sn-Pb solder joint creeps during thermal cycles between ambient and higher temperatures. Creep in Sn-Pb alloys proceeds via two mechanisms, dislocation climbing inside the grain matrix, and grain boundary sliding. The latter is the mechanism for superplasticity in Sn-Pb eutectic alloys. The work by Shine and et al [1,2] suggests that the fatigue life of a solder joint can be correlated to the amount of matrix creep during a thermal cycle, implying that the superplastic creep does not harm the fatigue resistance of the joint. It is important to understand the conditions for the superplastic creep in terms of temperature, stress, strain rate, and microstructural source.

Superplasticity in near-eutectic Sn-Pb alloys has been studied since the first published work by Jenkins in 1928.[3] He found that the cold-rolled alloys can be stretched under a prolonged tensile loading to an elongation of 410%, while the cast alloys have failed at elongations of only 10 to 20%. A later work by Pearson[4] showed that an extruded eutectic Sn-Pb wire can be slowly pulled up to 2000% at room temperature before rupture. This superplasticity was attributed to the stable, equiaxed microstructure that results from recrystallization at room temperature. Others [5-18] have explored the dependence of superplasticity in cold-worked Sn-Pb alloys on variables, such as testing temperature, grain size, stress, and strain rate. In contrast to the extensive studies on the cold-worked and

recrystallized Sn-Pb alloys, little attention has been paid to the alloys in the as-cast condition, beyond the repeated observation that as-cast alloys are not superplastic [3,4,6,19].

But the recent works by Solomon [20], and by Seyyedi, Arsenault, and Keller [21] have shown that as-solidified solder joints exhibit some superplastic characteristics: the stress exponent, n, in the relation, $\dot{\gamma} = A\ \sigma^n$, is between 2 and 3 in a certain strain rate range. Our recent work [22] has provided evidence for superplastic creep in the as-solidified solder joints in various aspects: stress exponent, activation energy, grain size effect, total amount of deformation, and the microstructure origin. This work is a continuation of our previous study, reporting new results on both creep tests and microstructural observations.

II. EXPERIMENTS

Since a detailed description of the experimental methods have been included in our previous paper [22], only the major points are mentioned here.

Specimen Preparation

A commercial 60/40 Sn-Pb solder paste was used, that is a blend of 80 wt % metallic powder and 20 wt % fully activated rosin flux.

The geometry and size of single and double shear specimens are shown in Fig. 1 where solder joints are sandwiched between the plates of printed circuit board that is made of epoxy fiber glass coated with a pure copper film. A pattern of 9 small squares, Fig. 1, of the copper film is produced by a process including applying a photoresist, electroplating Sn-Pb alloy, and etching off the copper. Three plates are assembled together with the aid of two through-thickness holes for alignment. Solder paste is placed with a pneumatic dispenser on each of 9 squares of the pattern before the three plates are packed. Sheathings are inserted between the plates to ensure a proper thickness for the solder paste. The plates are clamped and heated about 6 minutes in an oven at 208° C, above the liquidus of the 60/40 Sn-Pb (190° C), and then either cooled in air or quenched in a liquid nitrogen bath.

Creep Test

A creep test apparatus is schematically illustrated in Fig. 2. Both sides of the specimen are gripped by frictional gripping devices that consist of two steel plates with rough surfaces which can be tightened with socket screws. As shown in Fig. 2, the bottom part of the specimen is joined with the stand, and the top part is pulled by a weight pan via steel wire and pulleys. The displacement of the top part of specimen is monitored with a linear variable differential transformer (LVDT) that has a sensitivity of 9.63 mV output for a 25.4 μm (0.001") displacement. The output voltage signal is amplified and then is recorded by a personal computer through a 12 bit analog-to-digital converter. It is estimated that the creep device has a displacement resolution of at least 1 μm. Testing temperatures are achieved by immersing the specimens in a silicon oil bath with a temperature variation of less than 1°C.

Metallography

After the creep tests, the specimens were cut by a diamond blade saw to expose the solder joint cross section. The specimens were then cold-mounted, and prepared for microstructural observation by mechanic grinding and polishing with light pressure. The samples were final-polished with Mastermet (a colloidal silica polishing suspension) and etched with a solution of 25 ml distilled H_2O, 5 ml HCl (37% concentration), and 5 g of NH_4NO_3. The etching delineates the Sn grain boundaries in addition to providing contrast between the Sn-rich and Pb-rich phases. Optical microscopy at magnification of at least 1000x is necessary to observe the fine microstructure, and differential interference imaging is used to enhance the contrast between phases.

III. RESULTS AND DISCUSSION

Creep Tests

The steady state strain rate $\dot{\gamma}$ in a creep test can be expressed as functions of the applied stress τ, testing temperature T, and microstructure,

$$\dot{\gamma} = A\,\tau^n \exp\left(-\frac{\Delta H}{RT}\right). \qquad (1)$$

The stress exponent n and the activation energy ΔH reflect the creep deformation mechanism, and the pre-exponential factor A includes the microstructural effects. For a cold-worked and recrystallized Sn-Pb alloy, n varies with $\dot{\gamma}$ in a sigmoidal manner [7,8]. In the highest strain rate region, n is equal to or larger than 6 [7,11,13,14,17,18], in the intermediate $d\varepsilon/dt$ region, n reaches a minimum value that is close to 2 [5-18], and in the lowest $\dot{\gamma}$ region, n increases to 3.[12] Superplastic behavior is observed only in the intermediate $d\varepsilon/dt$ region where n = 2. The activation energy, ΔH, is approximately that of grain boundary diffusion when the alloy is superplastic [12,14,16,18], but changes to a value near that for self-diffusion at both higher [13,14,16,18] and lower [12] strain rates when superplasticity is lost. The strain rate in the superplastic region also depends highly on the effective grain size,[5,13,14,16,18] while the strain rate is independent of the grain size in normal creep at higher strain rates [13,14,16,18].

With this knowledge of creep behaviors of the recrystallized near-eutectic Sn-Pb alloys, our creep test results of the as-solidified solder joints can be presented as follows.

The stress exponent was determined in our previous paper by a stepped load creep test on a single specimen. In this method, a constant load is maintained until the strain rate reaches a steady-state value; the load is then changed to another level until another steady-state strain rate is obtained; and so on. The highest load is usually applied at the beginning of the test, and the load level decreased monotonically thereafter. With this method, a single specimen can generate four or five data pairs of stress vs. strain rate, while

conventional creep test requires many specimens to determine n in equation (1). The adoption of the stepped load method in our previous work was to minimize scatter in the data caused by specimen variation in solder joint contact area. However, the validity of the stepped load test method may be questioned. Since the microstructure may evolve during the deformation process, consequently, what may end up being tested at different loads is the same solder joint with different microstructures. Thus, conventional creep tests were used to verify the results of the previous stepped load creep tests.

Production of void-free solder joints with relative uniform joint contact area has been a problem, but with the improved techniques, enough void-free solder joints were made to perform the conventional creep tests to determine the stress exponents n. Typical creep test data of shear strain vs. time are plotted in Fig. 3. The creep curve has a slight primary creep stage, a roughly 15% shear strain of steady state creep stage, and a very long tail of tertiary stage. In Fig. 4, the steady state strain rate vs. the applied shear stress are plotted in double logarithmic scale. The tests were performed at 65° C mostly with single shear specimens for both air-cooled and liquid nitrogen quenched solder joints. A few double shear specimens were also tested. As seen in Fig. 4, at a strain rate of about 10^{-4} in/in per second, the slope of the $\log(\dot{\gamma})$ vs. $\log(\tau)$, i.e. the stress exponent n, changes from a value between 6 and 7 to a value of about 2; and at a strain rate of about 10^{-5} in/in per second, another change in n occurs from 2 to a value of about 3. The transition from 2 to 3 is not very clear, and is possibly due to scatter in the data. The transition in n implies a change in the deformation mechanism. At the higher strain rate above 10^{-4}, the deformation process is predominantly dislocation climbing, while at the lower strain rate, grain boundary sliding plays an important role.

As shown in Fig. 4, for $\dot{\gamma}$ above 10^{-4} in/in per second, the air-cooled solder joints crept at the same rate as the liquid nitrogen quenched solder joints with the same applied load; for $\dot{\gamma}$ below 10^{-4} in/in per second, the quenched solder joints crept faster than the air-cooled solder joints. The difference in creep rate at $\dot{\gamma}$ below 10^{-4} in/in per second can be explained by the difference in the microstructure. The quenched soldered joints have both fine grains, and fine Sn-rich and Pb-rich phases which promote the grain boundary sliding and rotation. The same phenomenon has been observed in bulk recrystallized eutectic Sn-Pb alloy specimens [13,14,16,18].

Fig. 5 shows the total shear deformation in creep before rupture as a function of the applied shear stress. The scatter in data is probably due to the joint geometry. It has been noticed that the total shear deformation depends on the solder pad area. However, in these creep-rupture tests, at high stresses and strain rates the total shear deformations were around 60%, while at low stresses and strain rates the total shear deformations were about 150%. The larger deformations at lower stresses and strain rates are related with the lower stress exponent at the lower stresses and strain rates. It has been proven in the superplastic theory that when n is equal to 1, the deformation can be infinite. In practical applications, superplasticity occurs when n is less than 3. The largest shear deformation before rupture obtained in these tests was about 300%. The creep test was performed at room temperature. A picture of this specimen before rupture is shown in Fig. 6.

In the previous study,[22] the stress exponent at lower stress and strain rate range was determined by the stepped load creep tests to be equal or less than 2. But in this study, the stress exponent at lower stress and strain rate range was measured by the conventional creep tests and found to be close to 3. The discrepancy is shown in Fig. 7. The small opened circles represent the stress vs. strain rate data from the conventional creep tests; while other symbols represent the data from the stepped load creep tests. In the lower stress and strain rate range, the strain rate form the conventional creep test was the slowest compared with the other strain rates determined by the stepped load tests for the same applied shear stress. The strain rates from the conventional creep test were determined from undeformed specimens reflecting the initial microstructure of the as-solidified solder joints. On the other hand, the strain rates determined from the stepped creep tests were measured with the specimens that had been deformed during previous load steps. The microstructure evolved during the deformation at 65° C that is 73% of the absolute liquidus temperature of 190° C for the 60/40 Sn-Pb solder.

The phenomenon of work softening has been reported [23,24] for a number of eutectic alloys, including Sn-Pb. The studies showed that eutectic Sn-Pb became softer in terms of hardness measurement after being hammered or rolled at room temperature. The phenomenon was attributed to recovery and recrystallization of the alloy at room temperature. However, metallographic confirmation was not fruitful. It is possible that in the stepped creep tests, the initial as-solidified microstructure of a solder joint is softened in the first load step, and results in a faster creep rate than that of an undeformed solder joint. The deformation promotes recrystallization which produces fine equiaxed grains, and in turn accelerates the grain boundary sliding process. The consequence of recrystallization is the reduction of the stress exponent from 3 for the initial microstructure to 2. However, recrystallization usually occurs only after a certain amount of deformation, but the amount of deformation seen in each stepped load is only about 5%. The factors that influence recrystallization in eutectic Sn-Pb, such as temperature, amount of deformation, and microstructure, are not well understood at this time.

There is an interesting example reported in the literature that is probably related to the softening phenomenon.[19,25] As shown in Fig. 8(a), the stress exponent of as-solidified eutectic Sn-Pb solder was determined by conventional creep tests to be equal to 6.[19] The same authors published the stress relaxation data as shown in Fig. 8(b).[25] Since the stress relaxation rate, $d\tau/dt$, is proportional to the strain rate, $\dot{\gamma}$, the slope in the double logarithm plot of $d\tau/dt$ vs. τ is the stress exponent n. It is seen in Fig. 8(b) that the slopes for the relaxation tests from a high initial strain (opened circles) change quickly from a high value to a value of about 2, and the slopes for the relaxation tests from a low initial strain change slowly from a high value to a value of about 3. The microstructure after deformation (as shown in Fig. 6 in ref. 25) exhibits equiaxed, recrystallized grains.

Microstructures

As reviewed in the Introduction section, previous studies on superplasticity in near eutectic Sn-Pb alloys have established that while the alloys are superplastic after being cold-worked and recrystallized, the initial as-cast alloys are not superplastic. However, recent

works on as-solidified solder joints indicate that the creep deformation in the joints exhibits some characteristics of superplasticity. Attempts have been made in this study to discover the microstructural origins for superplasticity in the as-solidified soldered joints. Since the superplasticity is usually related with stable, fine (< 5μm), and equiaxed grains, the effort has been in looking for this or a similar microstructure. The evidence has not been conclusive yet. However, in this report the microstructures produced in the various conditions, such as cold-worked, slow cooled, and quenched, are compared with that of as-solidified soldered joints, and the sources for the superplasticity in soldered joints are discussed.

The microstructure of a cold-worked 60/40 Sn-Pb alloy is shown in Fig. 9. A block of cast alloy was swaged into a rod (the deformation was more than 100%), and micrographs of transverse (Fig. 9(a)) and longitudinal (Fig. 9(b) cross sections were taken two days later after the alloy had been deformed and stored at room temperature. As seen in Fig. 9, the Sn-rich phase (light areas) has become equiaxed, while the Pb-rich phase (dark areas) has not. A probable explanation is that the Sn-rich phase has recrystallized, while the Pb-rich phase has not yet. The Sn-rich phase has an average grain size of about 3 μm.

The microstructures of a slowly cooled eutectic Sn-Pb alloy is shown in Fig. 10. The alloy was melted in a graphite crucible at 220° C, about 40° C above its melting temperature 183° C. The molten solder was taken out from furnace and cooled in air. The microstructure of this alloy shows the typical lammelar/colony features: the Sn-rich and Pb-rich phases are arranged side by side in long range, different oriented arrays form colonies. Figs. 10(a) and 10(b) show the microstructures inside a colony and on a colony boundary, respectively. The theory on solidification of the eutectic phase [26] states that there are preferred crystallographic interfacial relations between the eutecitic phases. A slowly cooled eutectic colony, to a first approximation, is two interpenetrating "single crystals", one of each phase, oriented with respect to each other. It is seen in Fig. 10(a) that the Pb-rich arrays are not perfect straight lines, they are slightly misoriented to each other, and in places a long narrow phase breaks up into several short pieces. Accordingly, the Sn matrix exhibits few grain boundaries to keep the interfacial relations with the less regular Pb-rich phase. On the other hand, in the colony boundaries the Sn-rich phase is mostly broken up, because both Pb and Sn-rich phase lamellas are heavily disturbed. The Pb/Sn and Sn/Sn boundaries inside a colony are not expected to accommodate grain boundary sliding, since they are either fixed boundaries or small angle boundaries. In contrast, the Sn/Sn boundaries and Sn/Pb boundaries on the colony boundaries are more or less movable. Transmission electron microscopy study of the eutectic Sn-Pb lamella [30] also indicated that the Sn matrix is not a monolithic grain but consists of polygranular grains. The study did not describe whether these grains had small angle or large angle boundaries.

The microstructure of a quenched 60/40 Sn-Pb alloy is shown in Fig. 11. The alloy was melted in a quartz tube and quenched in ice water. The Pb-rich phase particles are very fine. There are a few areas in Fig. 11 where fine lamellas are observable. The Sn/Sn grain boundaries are not visible even after repeated chemical etching.

The microstructures of quenched solder joints before testing are shown in Figs.12(a) and 12(b). The sizes of Pb-rich and Sn-rich phases (in Fig. 12(a)) are generally finer compared with that of slowly cooled, Figs 10(a) and (b). The morphology of Pb-rich and Sn-rich phases in quenched solder joints are not long range lamellar arrangement, compared with that of slowly cooled. Many areas in the joints, especially around the edges with copper interfaces, show equiaxed Sn-rich and Pb rich grains, Fig. 12(b). This equiaxed grains morphology is almost identical to that of recrystallized grain morphology, comparing Fig. 12(b) with 9(a).

The microstructure for quenched soldered joints after creep deformation is shown in Figs. 12(c) and 12(d). Note that many equiaxed, recrystallized Sn-rich and Pb-rich grains have developed around the crack. This is probably a similar phenomenon to that of the "coarsened bands" that have been reported in the study of thermal fatigue [27], isothermal fatigue [28], and creep [29] of the as-solidified eutectic Sn-Pb solder joints. However, the area that has equiaxed grains in this study does not shape into a long narrow band but is rather broad, and the equiaxed grains are much finer. This is probably due to the initial irregular microstructure that resulted from the rapid solidification rate.

IV. CONCLUSIONS

Based on the results of both creep tests and microstructure observations, it is concluded that the as-solidified solder joints exhibit some superplastic features because of their initial fine, and non-lamellar distribution of Pb-rich and Sn-rich phases; recrystallization occurs during creep deformation, which consequently softens the joints.

ACKNOWLEDGEMENTS

The authors are grateful to Mr. A. Kanzaki and Mr. R. Zink, Electronic Engineering Department, Lawrence Berkeley Laboratory, for their efforts in making creep test specimens. The valuable discussions with Dr. A. Sunwoo are greatly appreciated. This work is supported by Digital Equipment Corporation and by the director, Office of Energy Research, Office of Basic Energy Sciences, U.S. Department of Energy, under Contract NO. DE-AC03-76SF00098.

REFERENCE

1. M. C. Shine, L. R. Fox, and J. W. Sofia, *Brazing & Soldering*, 1985, No. 9, pp. 11-14.
2. M. C. Shine and L. R. Fox, Low Cycle Fatigue, ASTM STP, vol. 942, pp. 588-610, 1987.
3. C. H. M Jenkins, *J. Inst. Metals*, 1928, vol. 40, pp. 21-39.
4. C. E. Pearson, *J. Inst. Metals*, 1934, vol. 54, pp. 111-123.
5. D. H. Avery and W. A. Backofen, *Trans. ASM.*, 1965, vol. 58, pp. 551-562.
6. H. E. Cline and T. H. Alden, *Trans. AIME*, 1967, vol. 239, pp. 710-714.
7. P. J. Martin and W. A. Backofen, *Trans. ASM*, 1967, vol. 60, pp. 352-359.
8. S. W. Zehr and W. A. Backofen, *Trans. ASM*, 1968, vol. 61, pp. 300-313.
9. W. B. Morrison, *Trans. AIME*, 1968, vol. 242, pp. 2221-2227.
10. B. Baudelet and M. Suery, *J. Mater. Sci.*, 1972, vol. 7, pp. 512-517.
11. G. S. Murty, *J. Mater. Sci.*, 1973, vol. 8, pp. 611-614.
12. F. A. Mohamed and T. G. Langdon, *Philos. Mag.*, 1975, vol. 32, pp. 697-709.
13. D. Grivas, M.S. Thesis (1974) and Ph.D Thesis (1978), University of California at Berkeley.
14. D. Grivas, K. L. Murty, and J. W. Morris, Jr., *Acta Met.*, 1979, vol. 27, pp. 731-737.
15. A. E. Geckinli and C. R. Barrett, *J. Mater. Sci.*, 1976, vol. 11, pp. 510-521.
16. S. T. Lam, A. Arieli and A. K. Mukherjee, *Mater. Sci. Eng.*, 1979, vol. 40, pp. 73-79.
17. B. P. Kashyap and G. S. Murty, *Metall. Trans. A*, 1982, vol. 13, pp. 53-58.
18. B. P. Kashyap and G. S. Murty, *Mater. Sci. Eng.*, 1981, vol. 50, pp. 205-213.
19. D. Tribula and J. W. Morris, Jr., ASME Winter Annual Meeting 1989, San Francisco.
20. H. D. Solomon, *Brazing & Soldering*, 1986, No. 11, pp. 68-75.
21. J. Seyyedi, B. Arsenault, and J. P. Keller, Digital Equipment Corporation, *Soldering & SM Technology*, submitted, 1990.
22. Z. Mei, D. Grivas, M. C. Shine, and J. W. Morris, Jr., *J. Electronic Materials*, submitted, May, 1990.
23. F. Hargreaves, *J. Inst. Metals*, 1926, vol. 38, pp. 315-339.
24. F. Hargreaves and R. J. Hills, *J. Inst. Metals*, 1928, vol. 40, pp. 41-56.
25. D. Tribula, D. Grivas, and J. W. Morris, Jr., *J. Electron. Mater.*, 1988, vol. 17, pp. 387-390.
26. L. d. Graham and R. W. Kraft, *Trans. Met. Soc. AIME*, 1966, vol. 236, pp.94-102.
27. D. R. Frear, D. Grivas, and J. W. Morris, Jr., *J. Metals*, 1988, vol. 40, pp. 18-22. And *J. Electron. Mater.*, 1989, vol. 18, pp. 671.
28. D. Tribula, D. Grivas, D. R. Frear, and J. W. Morris, Jr., *Welding Research Supplement*, 1989, vol. 68, pp. 404s-409s.
29. T. S. E. Summers, and J. W. Morris, Jr., ASME Winter Annual Meeting 1989, San Francisco, J. of Electronic Pakaging, vol. 112, June 1990, pp. 94-9..
30. D. R. Frear, Chapter 4.1, Ph.D. Thesis, University of California, Berkeley, 1987.

FIGURE CAPTIONS

Fig.1 Double shear creep test specimen. Single shear specimen is made by cutting off one leg of the double shear specimen.

Fig.2 Schematic illustration of creep test apparatus.

Fig.3 Typical creep test curves.

Fig.4 Double logarithm plots of the steady state strain rate vs. shear stress data determined with conventional creep tests at 65° C on single shear specimens with air-cooled and liquid nitrogen quenched solder joints.

Fig.5 Rupture shear strain vs. applied shear stress.

Fig.6 A solder joint after being creep tested at room temperature, a total shear strain of about 300% was obtained.

Fig.7 Double logarithm plot of the steady state strain rate vs. shear stress data determined by both conventional creep tests (small opened circles) and stepped load creep tests (other symbols).

Fig.8 (a) the steady state strain rate vs. shear stress, and (b) the stress relaxation rate vs. shear stress of as-solidified eutectic soldered joint determined in Refs. 19 and 25, respectively.

Fig.9 Optical micrographs of a cold-swaged 60/40 Sn-Pb rod, in (a) transverse and (b) longitudinal cross sections.

Fig.10 Optical micrographs of a slowly solidified eutectic Sn-Pb alloy, (a) inside a colony, and (b) on a colony boundary.

Fig.11 Optical micrograph of a quenched 60/40 Sn-Pb alloy.

Fig.12 Optical micrographs of quenched 60/40 Sn-Pb soldered joints, (a) before creep test, for most areas, (b) before creep test in some edge areas.

Fig.12 The optical microstructures of quenched 60/40 Sn-Pb soldered joints, (c) after creep test, low magnification, and (d) after creep test, high magnification.

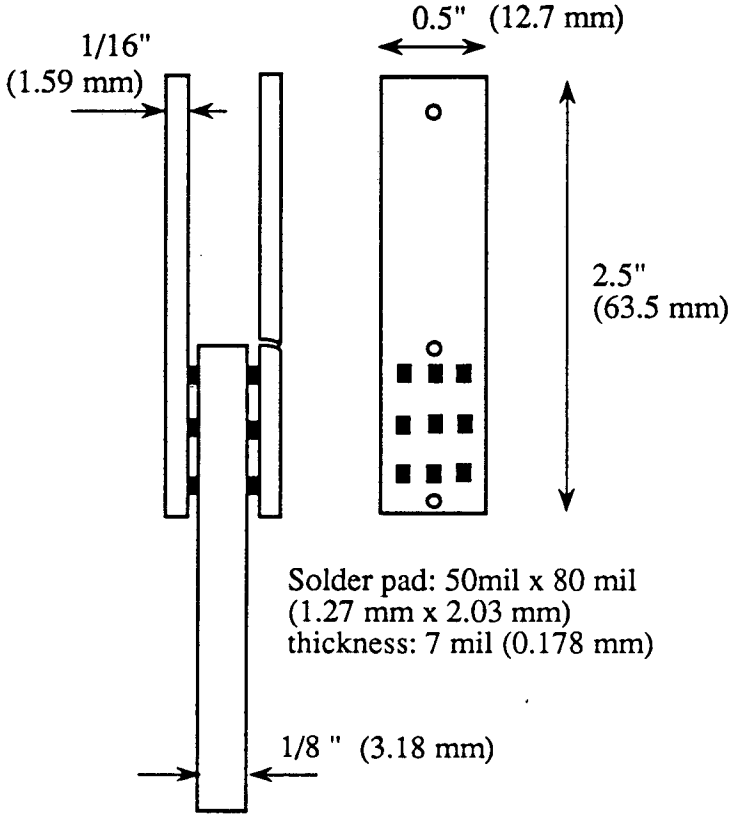

Fig. 1: Double shear creep test specimen. Single shear specimen is made by cutting off one leg of the double shear specimen.

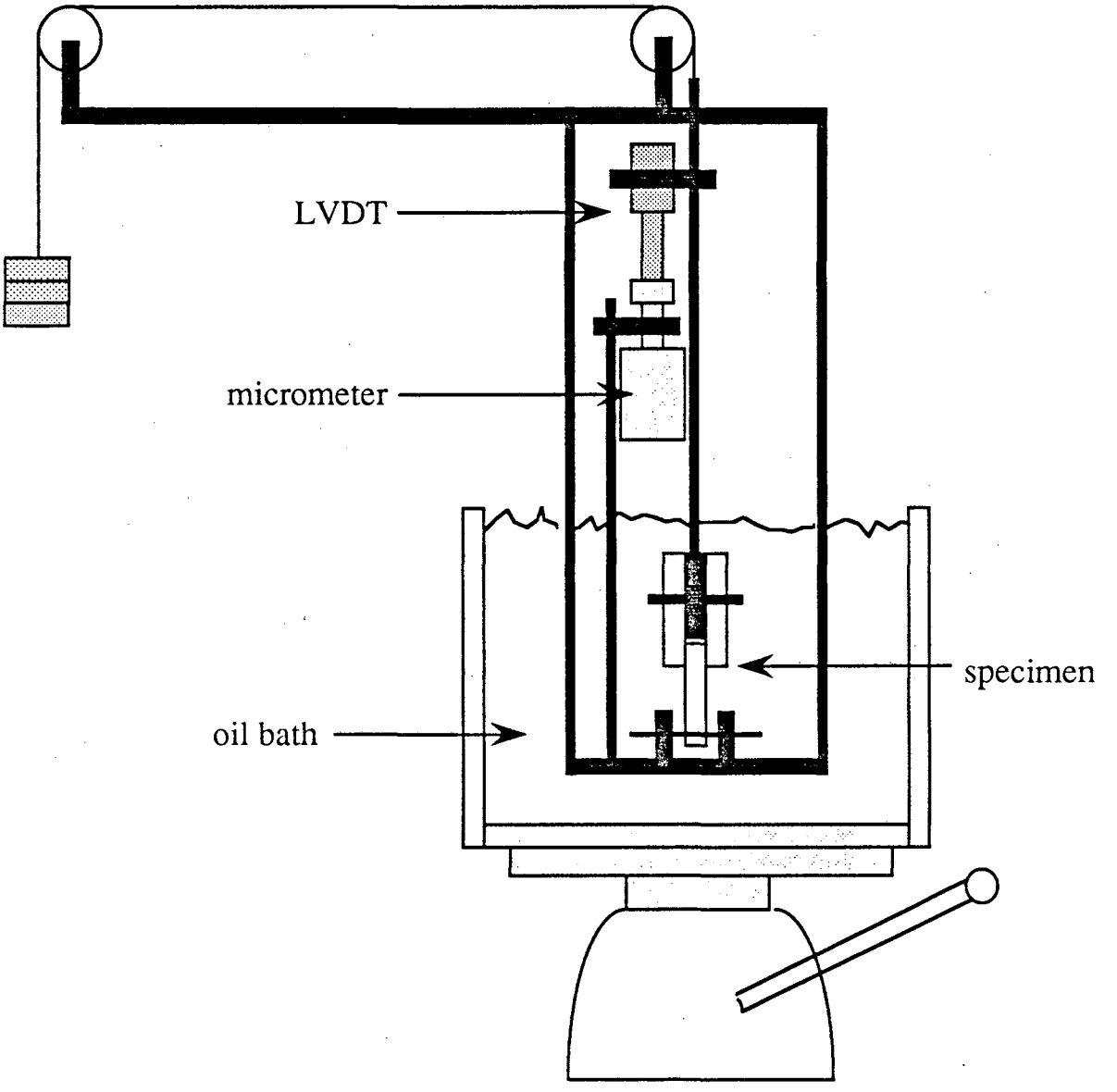

Fig. 2: Schematic illustration of creep test apparatus.

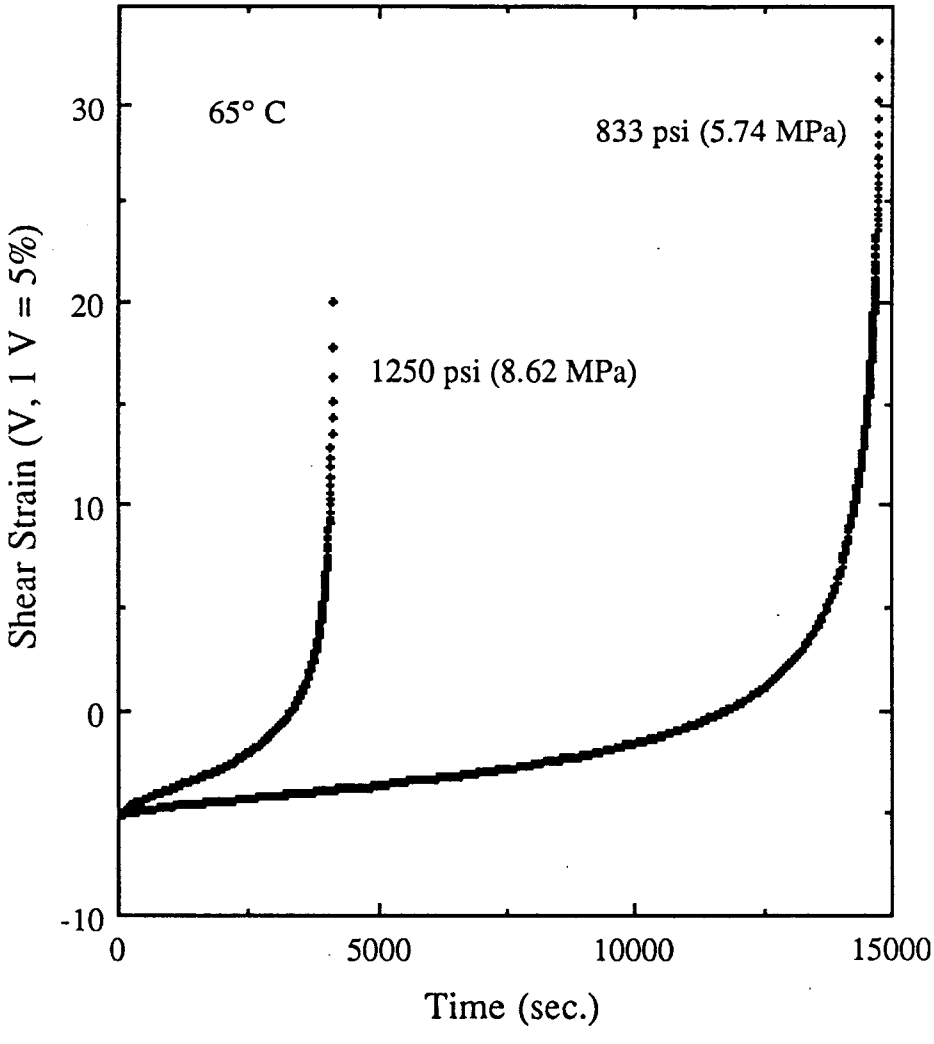

Fig. 3 Typical creep test curves

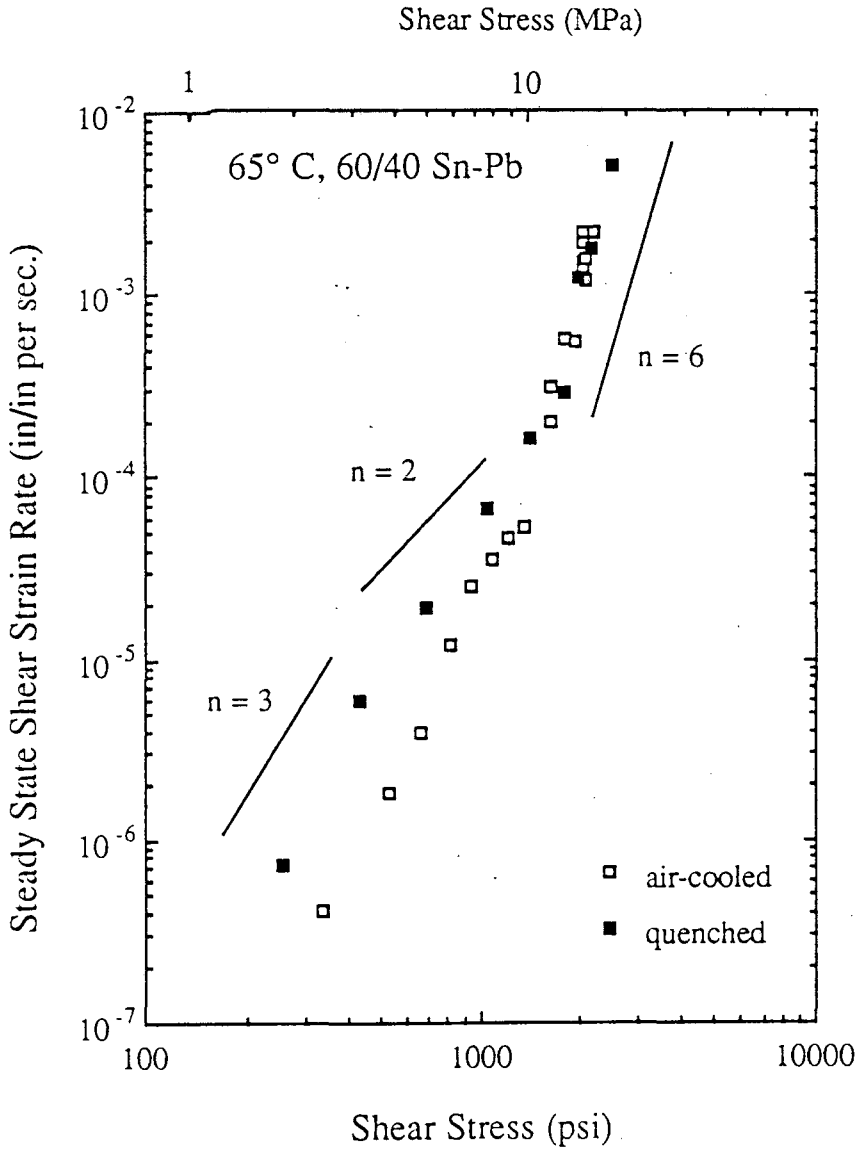

Fig. 4 Steady state shear strain rate vs. shear stress data determined at 65° C with air-cooled and liquid nitrogen quenched solder joints.

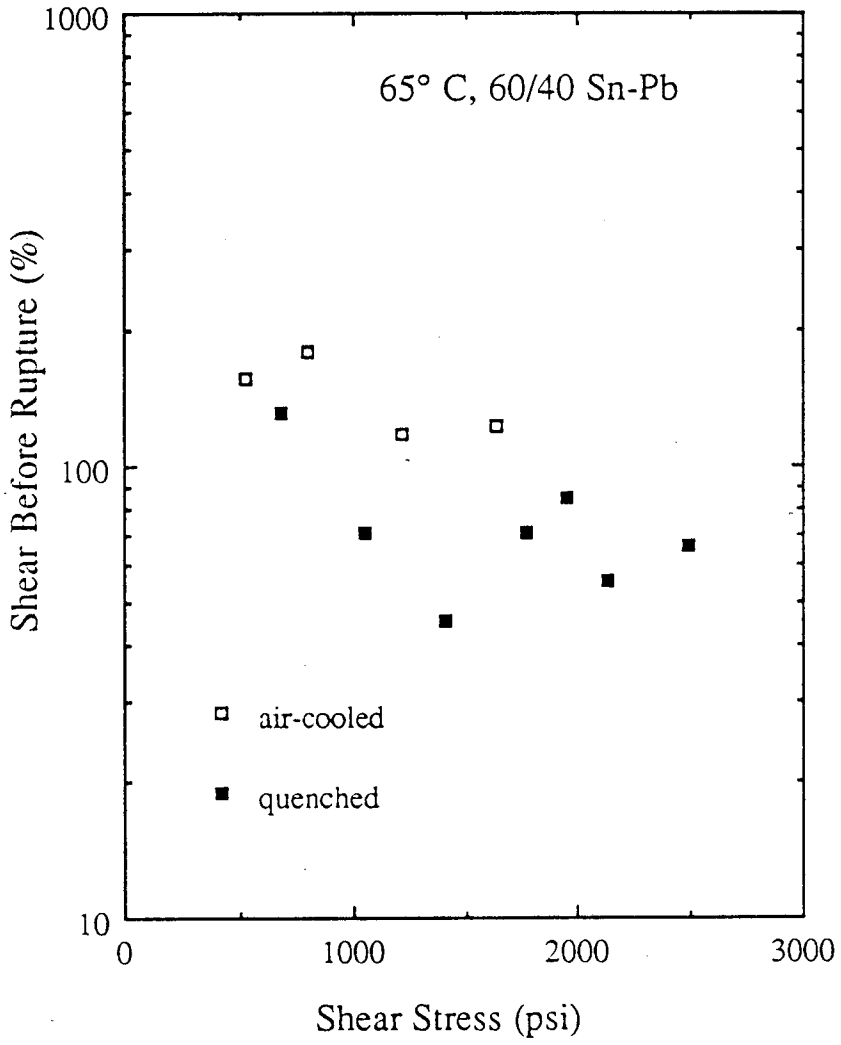

Fig. 5 Rupture shear strain vs. applied shear stress.

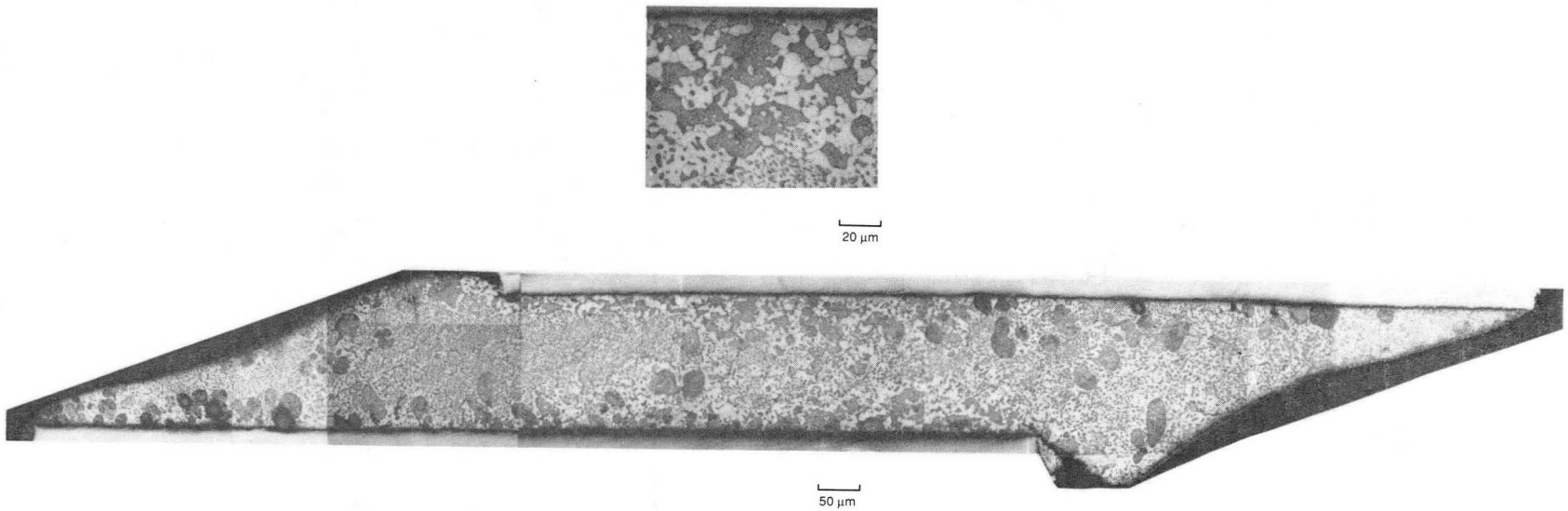

(XBB 896-5005)

Fig.6 A solder joint after being creep tested at room temperature, a total shear strain of about 300% was obtained.

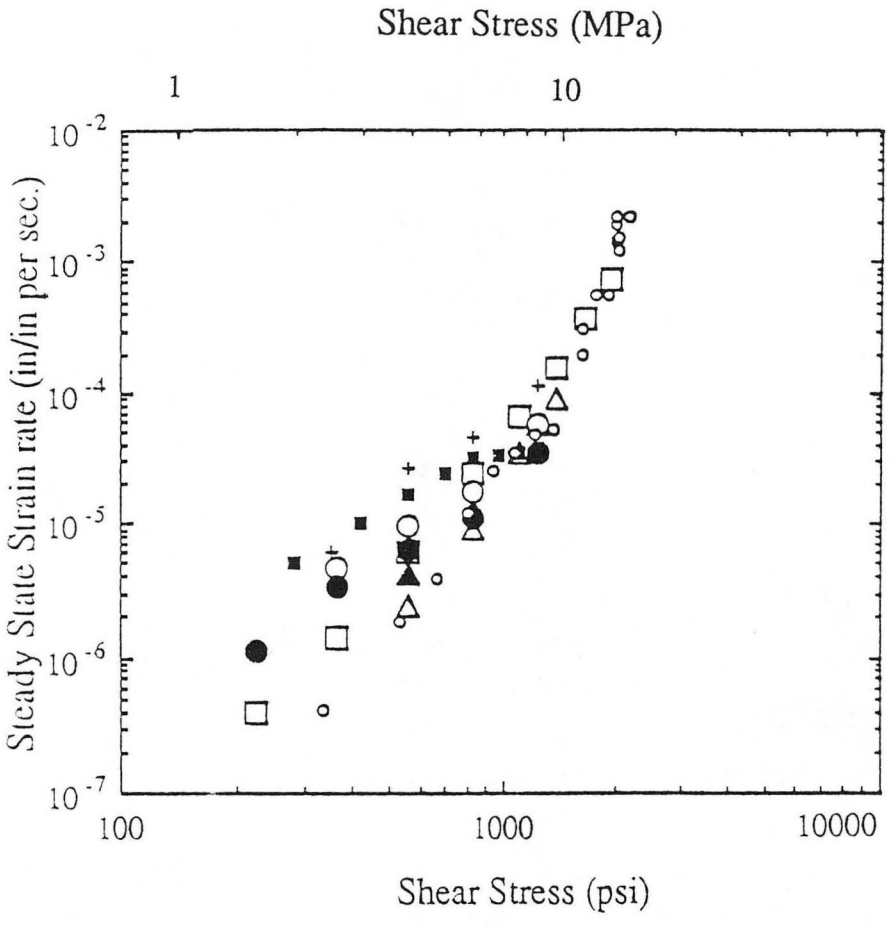

Fig.7 Double logarithm plot of the steady state strain rate vs. shear stress data determined by both conventional creep tests (small opened circles) and stepped load creep tests (other symbols).

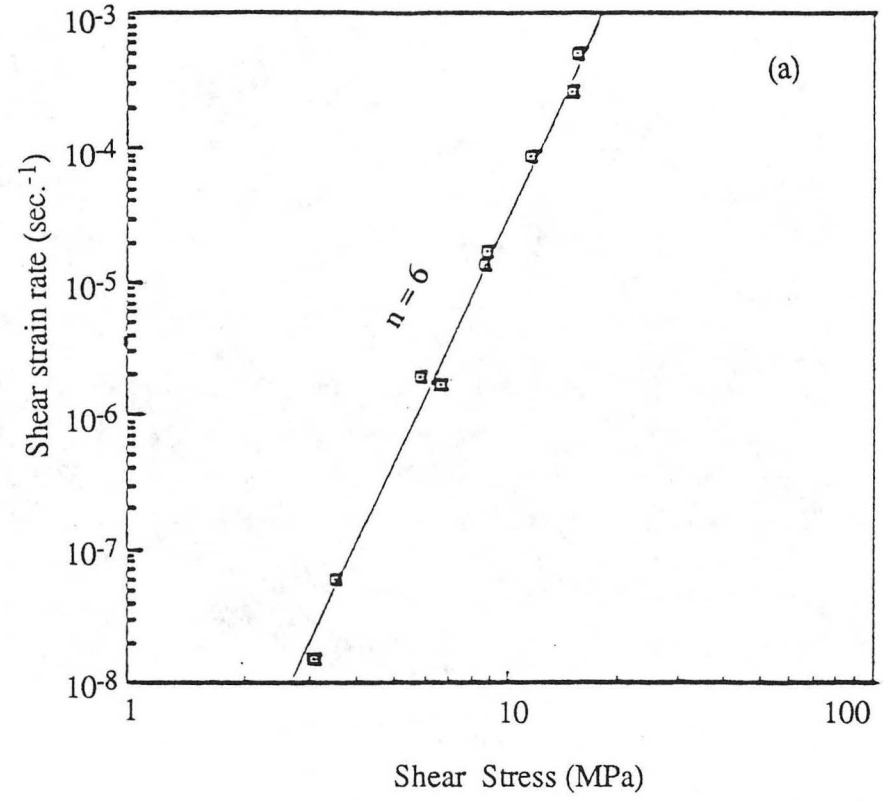

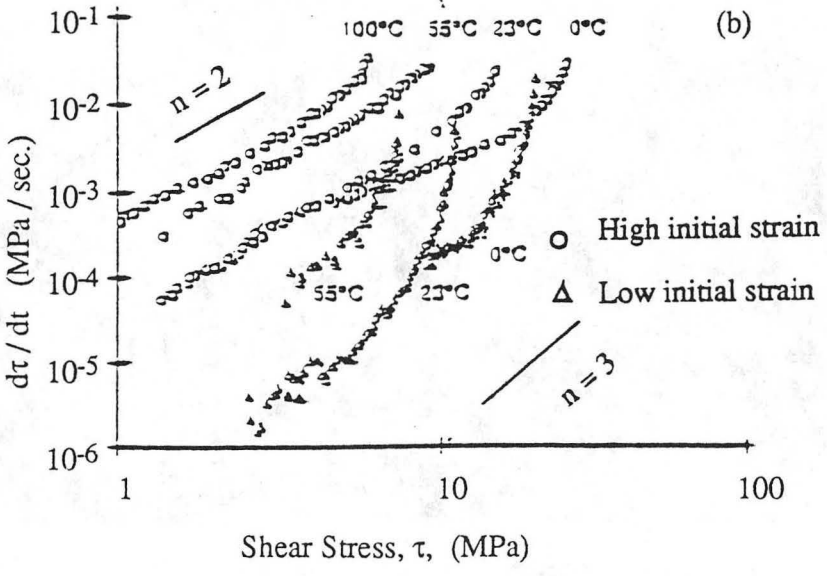

Fig. 8 (a) The steady state shear strain rate vs. shear stress, and (b) the stress relaxation rate vs. shear stress of as- solidified eutectic soldered joints determined in refs. 19 and 25, respectively.

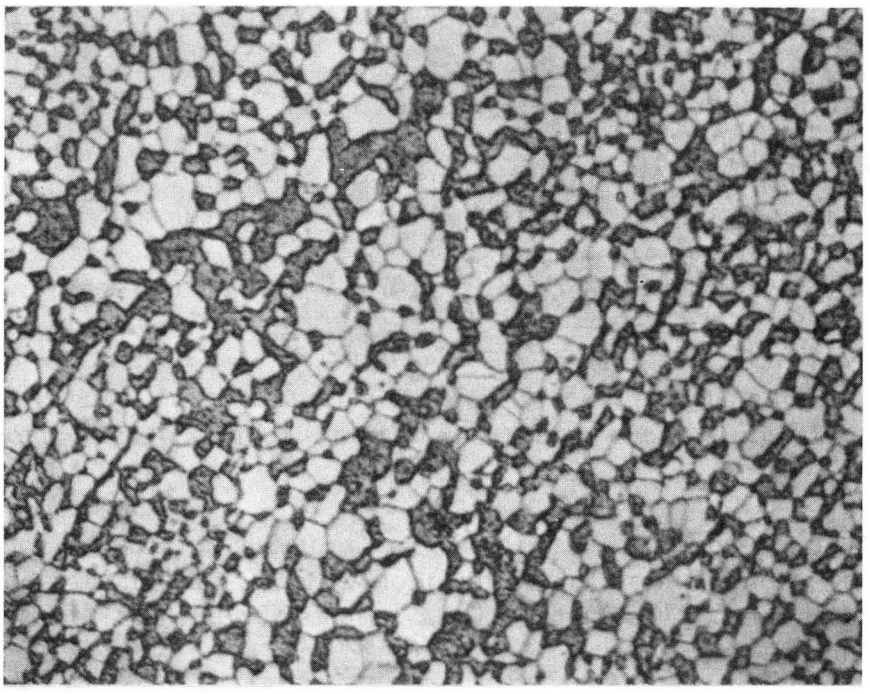

(a) (XBB 906-4854 top) 10 μm

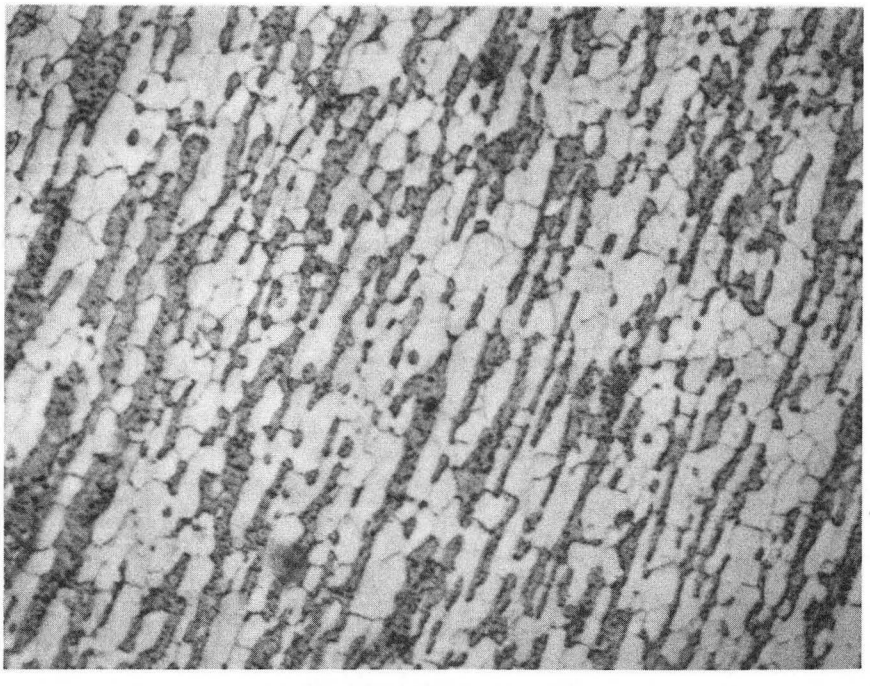

(d) (XBB 906-4854 bottom) 10 μm

Fig. 9 Optical micrographs of a cold-swaged 60/40 Sn-Pb rod, in transverse (a) and longitudinal (b) cross sections.

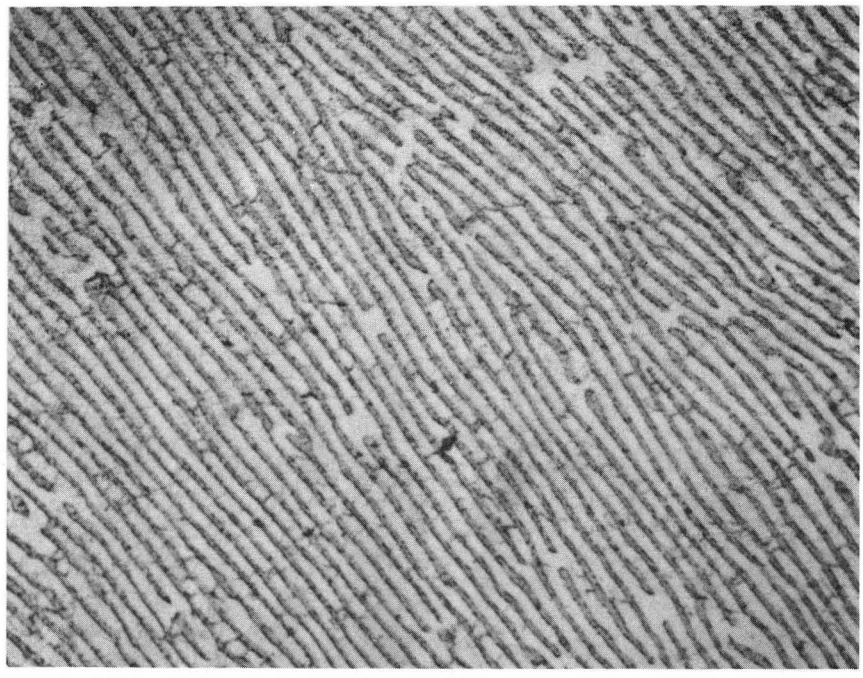

(a) (XBB 906-4857 top right) 10 μm

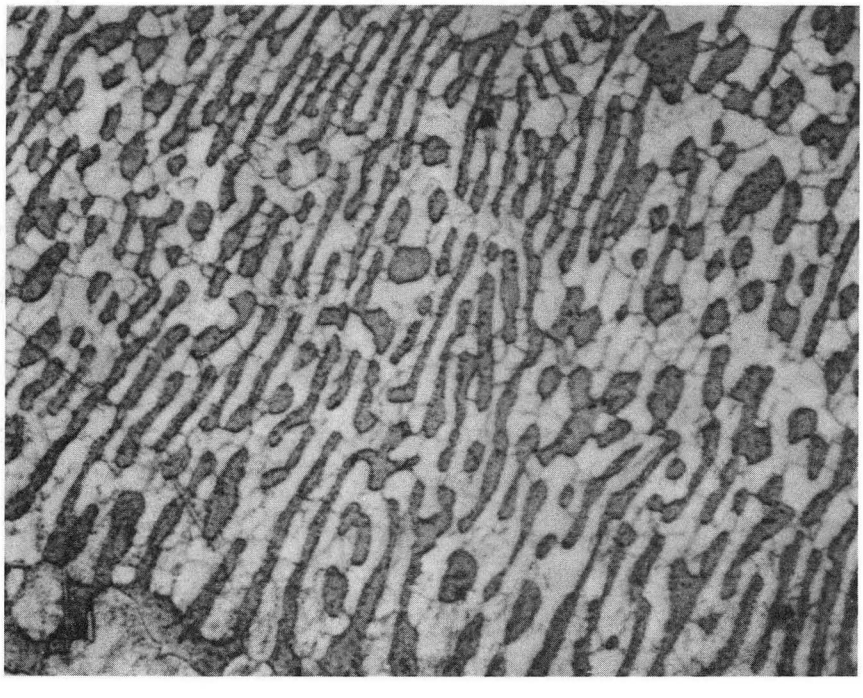

(b) (XBB 906-4856 bottom) 10 μm

Fig. 10 Optical micrographs of a slowly cooled eutectic Sn-Pb alloy, (a) inside a colony, and (b) on a colony boundary.

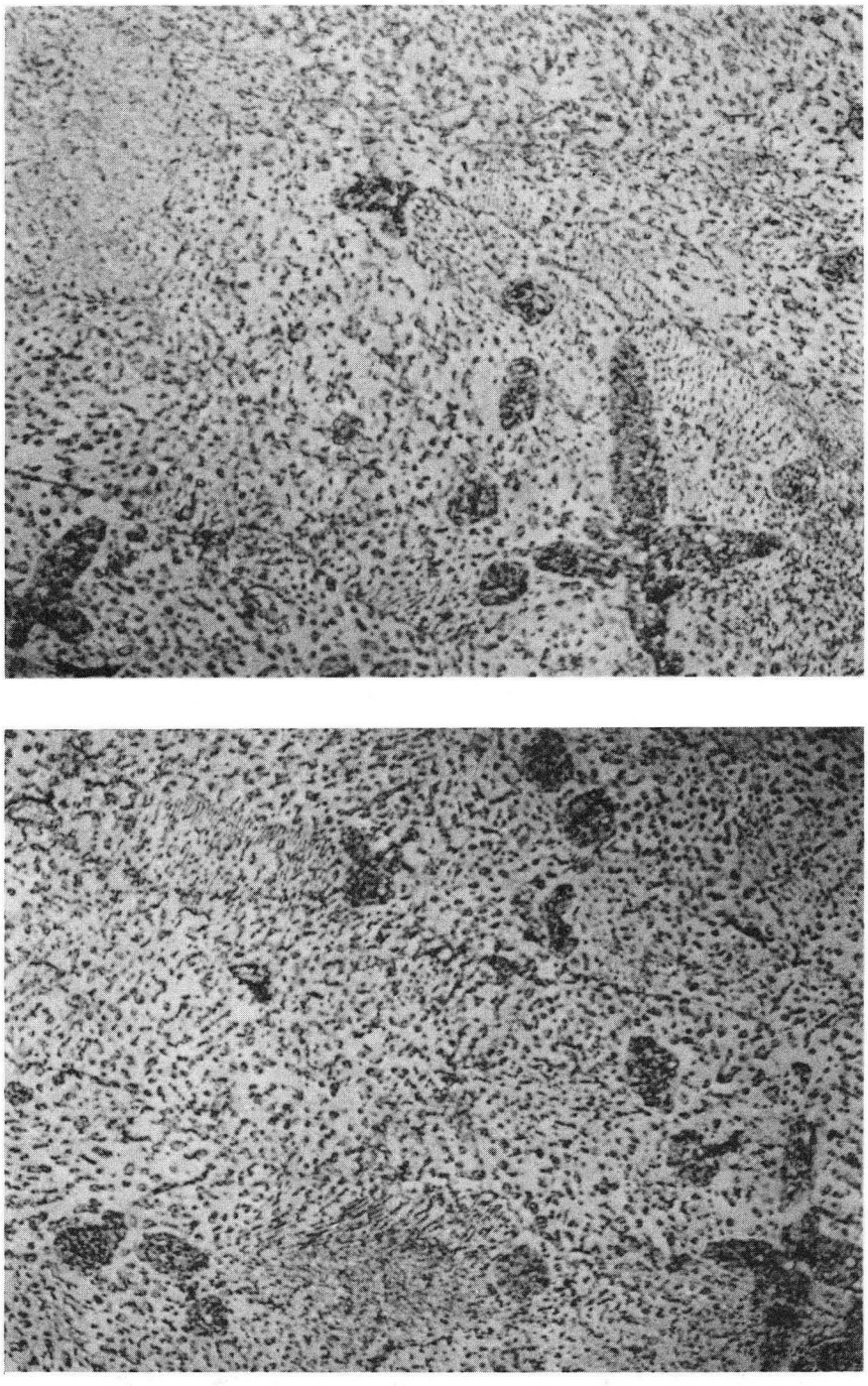

Fig. 11 Optical micrograph of a quenched 60/40 Sn-Pb alloy.

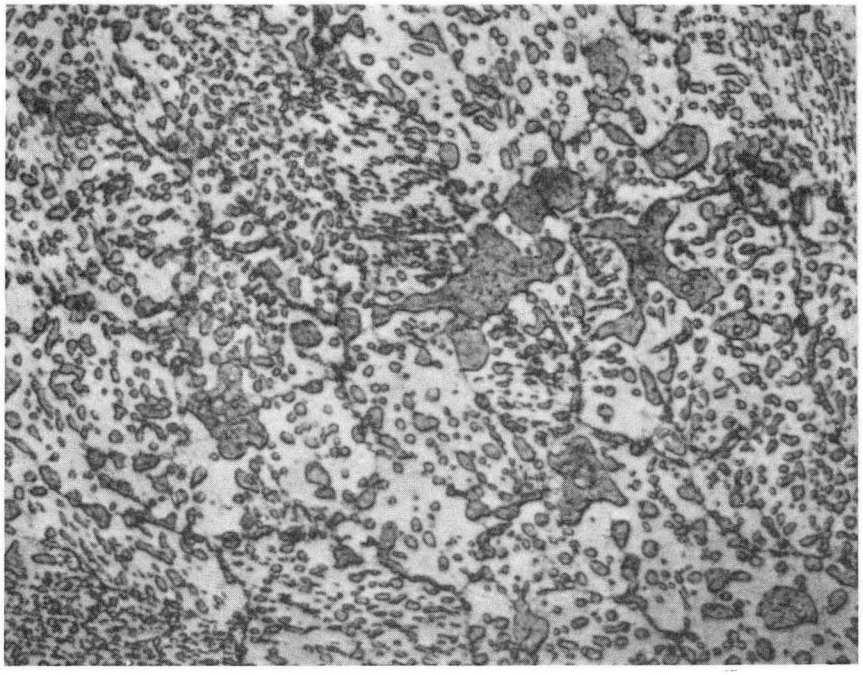

(a) (XBB 906-4853 bottom) 10 μm

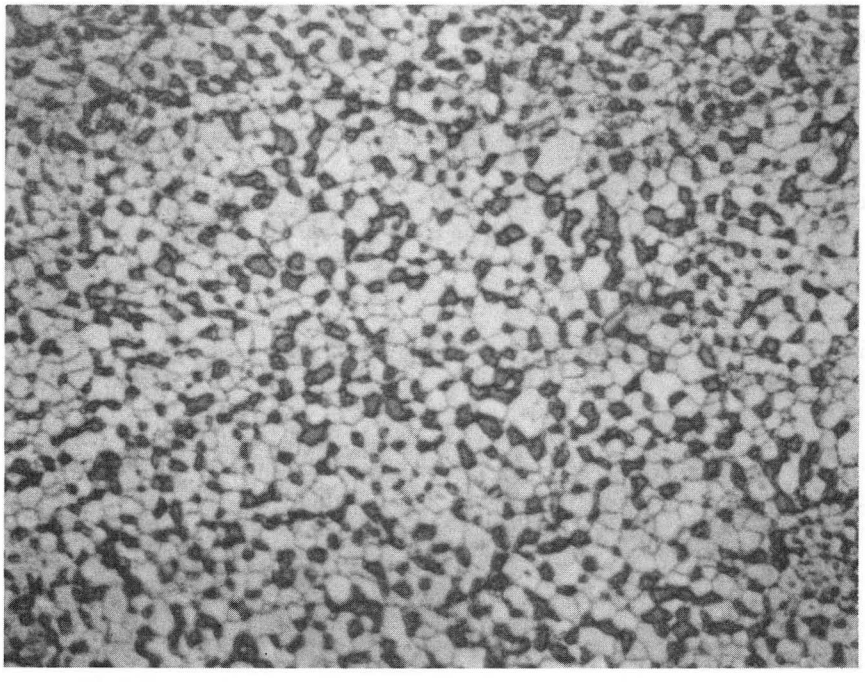

(b) (XBB 906-4853 top) 10 μm

Fig. 12 Optical micrographs of quenched 60/40 Sn-Pb soldered joints before creep test, (a) is most areas, and (b) in some edge areas.

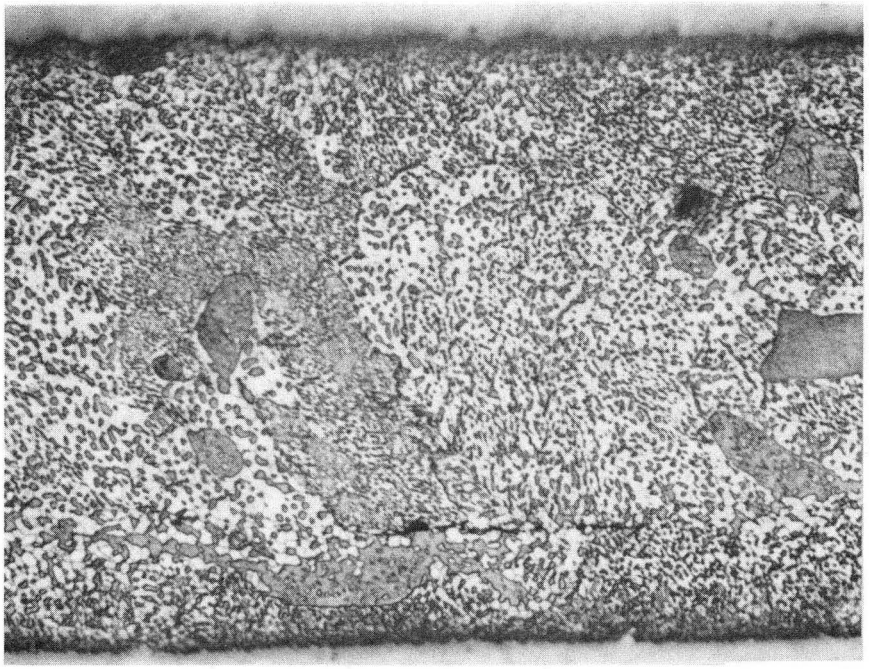

(c) (XBB 906-4851 bottom) 25 μm

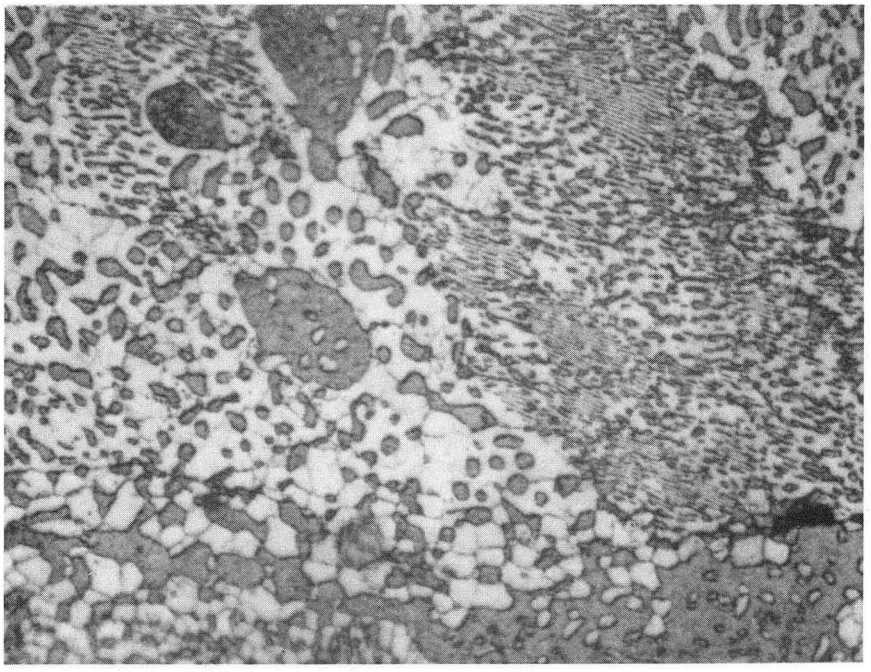

(d) (XBB 906-4850 bottom) 10 μm

Fig. 12 Optical micrographs of quenched 60/40 Sn-Pb soldered joints after creep test, (c) low magnification, and (d) high magnification.

LAWRENCE BERKELEY LABORATORY
CENTER FOR ADVANCED MATERIALS
1 CYCLOTRON ROAD
BERKELEY, CALIFORNIA 94720